Electrochimica Acta 437 (2023) 141536

Contents lists available at ScienceDirect

Electrochimica Acta

journal homepage: www.journals.elsevier.com/electrochimica-acta

Electrocatalytic hydrogenation and oxidation of glucose and xylose on mesoporous carbon-supported Au nanocatalysts

Jay Pee Oña [a], Rose-Marie Latonen [b], Narendra Kumar [a], Markus Peurla [c], Ilari Angervo [d], Henrik Grénman [a,*]

[a] Industrial Chemistry and Reaction Engineering, Johan Gadolin Process Chemistry Centre, Faculty of Science and Engineering, Åbo Akademi University, Henriksgatan 2, Turku FI-20500, Finland
[b] Laboratory of Molecular Science and Engineering, Johan Gadolin Process Chemistry Centre, Faculty of Science and Engineering, Åbo Akademi University, Henriksgatan 2, Turku FI-20500, Finland
[c] Institute of Biomedicin, University of Turku, Kiinamyllynkatu 10, Turku FI-20520, Finland
[d] Wihuri Physical Laboratory, Department of Physics and Astronomy, University of Turku, Turku FI-20014, Finland

ARTICLE INFO

Keywords:
Au nanocatalysts
Mesoporous carbon
Electrocatalysis
Hydrogenation
Electro-oxidation
Xylose
Glucose

ABSTRACT

Electrocatalytic conversion of hemicellulose-derived glucose and xylose presents a sustainable approach to utilize renewable energy (e.g. solar, wind) to produce value-added chemicals. In this work, the electrochemical hydrogenation and oxidation of glucose and xylose at ambient conditions were studied using dispersed, mesoporous Sibunit Carbon (SC)-supported Au nanocatalysts (SC/AuNPs) with different cluster sizes (4.4 nm, 5.9 nm, 10-30 nm), providing novel results on the cluster size - activity relation. For the electrocatalytic hydrogenation (ECH) of glucose and xylose into sorbitol and xylitol, respectively, higher conversion rates were obtained when more negative potentials were applied. This indicates that the hydrogenation reaction proceeds concurrently with hydrogen evolution reaction (HER). SC/AuNPs with smaller Au clusters were more active towards glucose or xylose ECH at all potentials applied. The selectivity (Faradaic efficiency) increased towards more negative potentials for glucose ECH but followed an opposite trend for xylose ECH. Analysis using *in-situ* FTIR-ATR spectroscopy showed that water adsorption which leads to HER, was more extensive in xylose solution than in glucose solution at lower potentials. This would indicate greater inhibition of xylose ECH than glucose ECH at more negative potentials. The electrocatalytic oxidation (ECO) of glucose and xylose to gluconic acid and xylonic acid, respectively, was observed to occur at -0.05, +0.3, and +0.4 V (vs Ag/AgCl) using the present electrocatalytic set up. Constant-potential electrolysis at these potentials showed differences in ECO rate depending on the applied potential and average Au cluster size. The highest glucose and xylose ECO rate was obtained for the SC/AuNPs with the smallest average Au cluster size (4.4 nm) at +0.3 V. Constant-potential electrolysis of the sugars at +0.3 V using this catalyst resulted in 42 % yield of gluconic acid and 32 % yield of xylonic acid in 6 hours, both with a very low Au loading of 0.08 % wt.. These results show the strong influence of Au cluster size on the catalytic activities of SC/AuNPs toward sugar ECH or ECO.

1. Introduction

The increasing pressure to replace fossil fuels with renewable sources of energy has prompted research to find ways to utilize this energy for sustainable production of fuels and chemicals. One major disadvantage of renewable energy sources (e.g solar, wind) is their intermittency, which primarily calls for reversible storage within the grid itself [1]. Another approach to solve this problem is to use secondary energy storage in the form of chemical bonds, which could maximize the utilization of renewable sources of electricity while providing a less energy intensive alternative for fuel and chemical production [1,2]. Electrocatalytic conversion provides a basis for this concept, and has been subject of studies in the last 20 years. Electrocatalytic transformations offer several advantages over conventional chemical processes such as operability in on aqueous feedstocks, elimination of external reducing or oxidizing reagents, and relatively milder reaction conditions.

Biomass is a viable platform for this process due to its abundance and

* Corresponding author.
E-mail address: henrik.grenman@abo.fi (H. Grénman).

https://doi.org/10.1016/j.electacta.2022.141536
Received 22 October 2022; Accepted 13 November 2022
Available online 14 November 2022

its amenability to electrochemical transformations. Electrocatalytic hydrogenation (ECH) of biomass-derived substrates is one way to upgrade feedstock either by increasing their H:C ratio or decreasing the O:C ratio through coupled deoxygenation/decarboxylation reactions [2]. This can be directly applicable to bio-oils to mitigate their intrinsic corrosiveness and chemical instability [3] as well as for lignin and hemicellulose valorization to produce fuels and chemicals [2,4]. ECH can be carried out at mild temperature and pressure compared to conventional thermocatalytic conversions. Moreover, hydrogen can be in-situ obtained from water splitting, thus eliminating the need for external supply of high-purity H_2 gas [5].

On the other hand, electrocatalytic oxidation (ECO) can be harnessed to produce added-value products from platform compounds such as glycerol [6–8], sugars [9–14], and furans [15–20]. ECO can be accomplished in solution at ambient conditions without external O_2 supply. The reaction conditions in both ECO and ECH can be readily controlled by the applied electric potential or current. These processes can be powered by renewable electricity, which serves as the basis for their sustainability in the context of valorization of biomass-derived feedstock [1].

Wood biomass contain 40-50 % cellulose and 15-30 % hemicellulose [21]. Extraction of hemicellulose can be accomplished by pressurized hot water or subcritical water extraction [22–24]. Depolymerization of hemicellulose via acid hydrolysis in batch or continuous mode [25–27] yields mainly glucose, xylose and mannose, which are raw materials for many chemicals. Glucose and xylose can be electrochemically converted over metal (electro)catalysts to produce added value chemicals. ECH of glucose and xylose would produce mainly sorbitol and xylitol, respectively, two widely used chemicals in the food, drug, and cosmetic industry [21]. On the oxidative side, ECO of glucose and xylose yields mainly gluconic acid and xylonic acid, respectively, both of which belong to the top-30 list of value added chemicals derived from biomass [28].

Reduction of glucose via ECH was earlier studied on Raney Ni catalyst [29,30], Pb [31], and Zn(Hg) [32]. Kwon and Koper studied ECH of glucose over a range of metals and identified late transition metals (Fe, Co, Ni, Cu, Pd, Au, and Ag) as having high selectivity towards sorbitol formation [33]. However, in the same study Pb gave the highest yield for sorbitol at higher overpotentials. ECH of xylose to xylitol was also demonstrated over amalgamated zinc catalyst in a divided electrocatalytic cell [34]. For most ECH studies on biomass-derived substrates, hydrogenation rates were found to be influenced by the functional groups present in the organic substrate [35,36], nature of electrode material [33,37], and reaction conditions (pH, temperature, solvent, electrode potential) [38]. In most electrocatalytic systems, ECH involves a chemisorbed hydrogen formed via the Volmer reaction (Eq. (1)) in aqueous solution upon

$$H_2O + e^- + M \rightarrow MH + OH^- \qquad (Volmer\ reaction) \tag{1}$$

$$M - C_xH_yO_z + 2MH \rightleftarrows 3M + C_xH_{y+2}O_z \tag{2}$$

application of negative potential:

The chemisorbed hydrogen can then react with an adsorbed substrate to form the hydrogenated product (Eq. (2)). Hydrogen evolution reaction (HER) also proceeds via the chemisorbed hydrogen intermediate through the Heyrovsky (Eq. (3)) and Tafel (Eq. (4)) reactions which significantly decreases the overall selectivity (Faradaic efficiency, *FE*) of the system.

$$2MH \rightleftarrows 2M + H_2 \qquad (\text{Tafel reaction}) \tag{3}$$

$$MH + H_2O + e^- \rightleftarrows M + H_2 + OH^- \qquad (\text{Heyrovsky reaction}) \tag{4}$$

On the other hand, the electrocatalytic oxidation (ECO) of glucose is well studied mostly for glucose fuel cells [10,39] and sensor applications [39–41]. Platinum and gold are two of the most studied catalysts for sugar electro-oxidation due to their high activities. However, surface poisoning has been observed in platinum possibly due to its ability to break C-C bonds, which also affects the overall selectivity. Gold nanoparticles (AuNPs) have been studied extensively for glucose oxidation due to enhanced catalytic activity and greater resistance towards surface poisoning than Pt in alkaline and neutral solutions [9,12,13]. ECO of sugars on alloys of gold were also investigated giving insights on the effect of metal ratio on product selectivity and catalyst stability [9,14]. The electro-oxidation of glucose and xylose are assumed to proceed via a two-electron transfer reaction described in Eqs. (5) and (6) [9]:

$$\text{Glucose}: C_6H_{12}O_6 + 3\ OH^- \rightarrow C_6H_{11}O_7^- + 2\ H_2O + 2\ e^- \tag{5}$$

$$\text{Xylose}: C_5H_{10}O_5 + 3\ OH^- \rightarrow C_5H_9O_6^- + 2\ H_2O + 2\ e^- \tag{6}$$

In this work, the electrocatalytic conversion of glucose and xylose, two main components of wood hemicellulose, was investigated using gold nanocatalysts in a divided electrolytic cell at ambient conditions. Gold was chosen as catalyst due to its aforementioned activity towards both sugar ECH and ECO. The influence of Au cluster size on electrocatalytic conversion of glucose and xylose was investigated. We have previously observed that sugar ECH rates were higher for carbon fiber-supported Au nanocatalysts than for polycrystalline Au electrocatalyst [42]. However, conventional methods for depositing Au on carbon such as deposition-precipitation produce typically large clusters of gold [43]. Hence, deposition of pre-reduced gold from gold sols on mesoporous carbon support was employed for obtaining higher dispersion and better control of the nanoparticle size. AuNPs size control can be achieved by varying the ratio of the gold precursor (i.e. $HAuCl_4$) and the poly(vinyl alcohol) (PVA) in the prepared sols [43]. The presence of protective agents (e.g. pol(vinyl alcohol)) in gold sols prevents the aggregation of the formed AuNPs both in solution and presumably on the catalyst support, thus allowing to obtain a well-dispersed Au nanocatalyst [43,44].

The catalyst support used in this study is Sibunit Carbon (SC), a type of mesoporous carbon obtained by depositing pyrolyzed C_1-C_4 hydrocarbons on granulated carbon black [45]. Due to its desirable properties as a catalyst support, such as high purity and mechanical strength, chemical stability and reasonably large surface area, catalytic studies involving SC have increased in number in the last 30 years [46–49]. To the best of our knowledge, SC-supported metal catalysts have not been studied in the electrocatalytic conversion of platform chemicals for biomass valorization. Its high surface area and relatively large pores make SC an ideal catalyst support for the conversion of high molecular weight compounds such as sugars.

The synthesized SC-supported AuNPs (SC/AuNPs) were characterized using physico-chemical and electrochemical methods, and their properties were correlated with their electrocatalytic activity. To the best of our knowledge, the effect of AuNPs size on the activity towards sugar ECO has not previously been demonstrated for supported Au nanocatalysts. Moreover, the dependence of the catalyst activity on the AuNPs cluster size towards glucose and xylose ECH was explored in this work for catalysts with narrower AuNPs size distribution compared to our previous study [42], which also improves the insight in the results. Aside from the physical properties of the catalyst, the effect of applied potentials on the activity and selectivity of the hydrogenation and oxidation reactions was also investigated.

2. Experimental

2.1. Materials

Hydrogen tetrachloroaurate (III) hydrate (49 % Au) was obtained from Alfa Aesar/ABCR GmbH. D-glucose (BioUltra, ≥ 98% wt.), D-xylose (BioUltra, ≥ 99% wt.) and poly(vinyl alcohol) (PVA, 99+% hydrolysed, Mw = 89,000-98,000) were obtained from Sigma-Aldrich. The carbon felt (≥ 99.0 %) used to prepare the working electrodes

was purchased from Alfa Aesar. All other chemicals were of analytical grade. Deionized water (resistivity 18 MΩ-cm) was used to prepare all solutions.

2.2. Catalyst preparation

The catalysts were prepared by depositing AuNPs from gold sols onto SC. The gold precursor - hydrogen tetrachloroaureate ($HAuCl_4$) was dissolved in deionized water to make initial concentrations of 60, 80, and 120 μg/mL. Under vigorous stirring, 1.25 mL of 2% wt. PVA was added dropwise to 160 mL of each $HAuCl_4$ solution. Afterwards, 132 mL of freshly prepared 0.1 mol L^{-1} $NaBH_4$ solution was added dropwise to the mixture. After a few minutes, gold sol was immobilized on SC by adding an appropriate amount of the support to the mixture under constant stirring. The nominal Au loading was 5 % wt. After 2 h stirring the slurry was filtered under vacuum and the catalysts were thoroughly washed with hot deionized water. SC-supported AuNPs (SC/AuNPs) were thus obtained. The SC/AuNPs catalysts were then dried overnight at 60 °C in an oven. Three kinds of SC/AuNPs catalysts were prepared based on the initial $HAuCl_4$ concentrations and the resulting PVA/Au and $NaBH_4$/Au ratios are summarized in Table S1.

2.3. Catalyst characterization

Nitrogen physisorption was carried out using the MicroActive 3Flex™ 3500 (Micromeritics) sorptometer to calculate the specific surface area and the pore volume of the SC/AuNPs catalysts. Prior to analysis, the catalysts were outgassed for 5 h at 180 °C. The specific surface area was calculated from the Dubinin-Radushkevich equation, whereas the pore volume and pore size distribution were estimated from the Horvath and Kawasaki method.

Scanning electron microscopy/Energy disperse X-ray Analysis (SEM/EDXA) was used to study the surface morphology and estimate the gold content of the synthesized SC/AuNPs catalysts. The instrument was a Leo Gemini 1530 scanning electron microscope with a Thermo Scientific UltraDry Silicon Drift Detector. The AuNPs sizes were measured using transmission electron microscopy (TEM) using a JEOL JEM 1400 Plus electron microscope operated at 120 kV acceleration voltage and 0.38 nm resolution. The gold content of the SC/AuNPs catalysts were determined from Inductively coupled plasma-optical emission spectrometry (ICP-OES) analysis (Varian Liberty 110 ICP Emission Spectrometer). Samples for ICP-OES analysis were prepared by dissolving of 0.10-0.14 g of catalyst in 50 mL concentrated H_2SO_4 and digested in a microwave heater at 150 °C. The resulting solutions were diluted to 100 mL and taken for analysis.

X-ray powder diffraction (XRD) was used to analyse the structural properties of the catalysts. The instrument was a PANalytical Empyrean X-ray powder diffractometer with Cu LFF X-ray tube. X-ray radiation was filtered to include only Cu $K_{\alpha1}$ and Cu $K_{\alpha1}$ components. XRD data were processed using the MAUD (Material Analysis Using Diffraction) analysis program.

2.4. Electrochemical measurements

Activity and electrochemical surface area measurements were carried out using linear sweep voltammetry (LSV) and cyclic voltammetry (CV). The general electrochemical set-up consisted of a three-electrode system in an H-shaped electrochemical cell divided by a Nafion 117 membrane (Ion Power, Inc.). The potential was supplied by an Autolab (PGSTAT100) General Purpose Electrochemical System at room temperature (23 ± 1 °C). Before the experiments, the electrochemical cell was cleaned by immersing in a 1:1 mixture of sulfuric and nitric acid overnight and boiling in ultrapure water (resistivity 18 MΩ-cm). Pretreatment of the Nafion membrane involved boiling in H_2O_2 solution (3 % vol.) for 1 h and in sulfuric acid (2 mol L^{-1}) for 1 h, with thorough rinsing in deionized water in between the boiling steps. The reference electrode used was Ag/AgCl/3M KCl (Thermo Scientific Orion™ 900100). All the potentials were measured against this Ag/AgCl/3M KCl reference electrode. The counter electrode was constructed by attaching activated carbon fibers (3.0 cm^2 area, 0.60 mm thickness, Kynol®) to a carbon rod (99.999% carbon, Strem Chemicals Inc.). The SC/AuNPs working electrode was constructed by preparing a catalyst ink and dropcasting on a carbon felt. The catalyst ink was prepared by dispersing 10 mg of SC/AuNPs in 1 mL deionized water and 1.5 mL of isopropanol. The mixture was then sonicated for 30 mins. Afterwards, the catalyst ink was applied to the carbon felt (2 cm x 1.5 cm) by dropcasting and was dried overnight at room temperature. The resulting SC/AuNPs electrode had a geometric area of 6 cm^2.

LSV and CV were carried out in the H-shaped electrochemical cell (Latech) separated by a Nafion membrane (Ion Power, Inc.). The working and reference electrodes were contained in the same compartment while the other compartment held the counter electrode. Both compartments contained the same electrolyte solution during the electrochemical experiments. Glucose or xylose was dissolved into the supporting electrolyte solution (0.1 mol L^{-1} Na_2SO_4 or 0.1 mol L^{-1} NaOH) to make a concentration of 0.1 mol L^{-1}. The sugar solutions were initially purged with N_2 for 15 min and the N_2 gas was kept above the solution during all electrochemical characterization experiments. For the LSV experiments, the potential was swept from 0 to -1.5 V at a scan rate of 5 mV s^{-1}. On the other hand, CV was carried out by cycling the potential between -0.8 V to 0.8 V at a scan rate of 10 mV s^{-1}. Current densities were normalized to the electrochemically active surface area (ECSA) of the working electrode.

The ECSA of each SC/AuNPs electrode was estimated from the charge of gold oxide reduction. CV measurements were carried out in the H-shaped electrochemical cell using 0.5 mol L^{-1} H_2SO_4 as supporting electrolyte. The potential on the SC/AuNPs electrode was cycled between 0 and 1.5 V (vs Ag/AgCl) at a scan rate of 1 mV s^{-1}. The charge of gold oxide reduction was calculated between 0.7 and 1.1 V. The charge density value used to calculate the ECSA was 390 μC cm^{-2}, corresponding to the reduction charge for one monolayer of AuO per unit area.

2.5. In-situ FTIR-ATR Spectroscopy

ECH of glucose and xylose over Au catalyst were investigated by Fourier transform infrared (FTIR) attenuated total reflectance (ATR) spectroscopy. The spectra were recorded on a Bruker IFS 66/S FTIR instrument equipped with an MCT detector. Gold was sputtered on the ZnSe reflection element (10 mm x 10 mm x 2 mm) with a layer thickness of 40 nm. The ZnSe/Au electrode was attached to a small spectroelectrochemical flow-through cell made of Teflon. The reference electrode was an Ag/AgCl wire and the counter electrode was a Pt coil. A beam condenser 4XF-BR3 (Harrick Scientific) served as the attachment to the FTIR spectrometer. The spectra were recorded in the range between 4000 to 400 cm^{-1} with a resolution of 8 cm^{-1} and 200 interferograms were co-added. Spectra were recorded from 0 V to -1.3 V at 0.1 V intervals. Each potential was applied for 10 minutes, after which the spectrum was obtained. The measured spectra were related to a reference spectrum recorded after the first minute of application of 0 V for both glucose and xylose solutions. The spectra shown in this work therefore describe the spectral differences from the reference state.

2.6. Electrocatalytic conversion of glucose and xylose

Constant-potential electrolyses were carried out to determine the activity and *FE* of the SC/AuNPs catalysts toward the electrocatalytic reduction/oxidation of glucose and xylose. For these experiments, the three-electrode set-up in the H-shaped electrochemical cell configuration was employed. The SC/AuNPs working electrode was prepared as described in 2.4. For the glucose or xylose ECH, the working and reference electrodes were immersed in 25 mL of 0.1 mol L^{-1} Na_2SO_4

with 0.1 M glucose or xylose. The counter electrode (activated carbon fiber attached to carbon rod) was placed in the anodic compartment containing 25 mL of the supporting electrolyte solution (0.1 mol L^{-1} Na_2SO_4). On the other hand, for glucose or xylose electro-oxidation, the SC/AuNPs electrode and reference electrode were immersed in a solution of 0.1 mol L^{-1} NaOH with 0.1 M glucose or xylose. The opposite compartment contained the counter electrode immersed in 0.1 mol L^{-1} NaOH. The designated potentials were supplied by the Autolab (PGSTAT100) potentiostat for a specific duration and samples were collected from the reaction solution thereafter. During electrolysis the reaction solution was stirred at approximately 300 rpm to facilitate the mass transport of the sugar to the working electrode.

2.7. Product analysis

Samples were collected from the reaction solution after the constant-potential electrolyses and analysed using High-performance liquid chromatography (HPLC) with a refractive index detector. The HPLC column used was an Aminex HPX-87C kept at 80 °C and the eluent was 1.2 mM $CaSO_4$ solution. Prior to analysis, the pH of the samples were adjusted to pH 7 using either dilute NaOH or H_2SO_4. Afterwards, 1 mL of sample was passed into a strong anion and cation exchange SPE tubes (Supel™, Merck) to remove excess ions from the supporting electrolyte.

3. Results and discussion

3.1. Catalyst characterization

Mesoporous carbon-supported Au nanocatalysts were prepared by depositing AuNPs from gold sols on SC. SC powder is composed of granules (0.5-25 μm, Fig. S8) with high carbon purity determined from EDXA (Fig. S9). The cluster size of the AuNPs was controlled by varying the concentration of the gold precursor ($HAuCl_4$) while maintaining the amount of the reductant ($NaBH_4$) and stabilizing agent (PVA) constant. ICP-OES analysis of the resulting catalysts confirmed the deposition of gold on SC. The actual gold content of the catalysts measured by ICP-OES were significantly lower than the nominal Au loading of 5 wt. % as shown in Table 1.

This is possibly due to the high stability of AuNPs in the gold sol and the weak interaction between the AuNPs and the surface functional groups on the support (SC). The gold nanoparticle size measured using TEM (Fig. 1) revealed differences in AuNPs sizes resulting from different concentrations of the gold precursor ($HAuCl_4$) used. As listed in Table 1, the SC/AuNPs-A catalyst with lowest concentration (60 μg/mL) of the precursor yielded the smallest average Au nanoparticle size (4.4 nm). The largest Au cluster sizes (10~30 nm) was measured for SC/AuNPs-C synthesized with the highest $HAuCl_4$ concentration (120 μg/mL). As seen in Fig. 1, the AuNPs in SC/AuNPs-A and SC/AuNPs-B were widely dispersed throughout the surface of the SC support while the AuNPs in SC/AuNPs-C formed aggregates aside from dispersed nanoparticles. A closer look at the Au clusters in SC/AuNPs-C shows that they were formed from aggregates of AuNPs with sizes of about 10-30 nm (Fig. S6). These results show that an optimum PVA/Au (wt/wt) ratio of 5 (Table S1) was necessary to avoid the aggregation of the resulting AuNPs and obtain higher dispersion and narrower size distribution.

The Au dispersion (D_{Au}) was estimated from the average Au cluster size (d) using the following formula [50]:

$$D_{Au} = \frac{6M}{d\rho a_{Au} N_A} * 100\% \quad (7)$$

where M corresponds to the molar mass of Au (0.197 kg/mol), ρ is the density of gold (1.932×10^4 kg/m^3), a_{Au} is the effective surface area of one Au atom (8.7×10^{-20} m^2), and N_A is the Avogadro number. Eq. (7) describes an inverse relationship between the dispersion and Au cluster size, which was then reflected in the Au dispersion values in Table 1.

The X-Ray diffraction results for SC/AuNPs-A, SC/AuNPs-B, and SC/AuNPs-C catalysts are shown in Fig. 2. All the diffractograms show a broad peak close to 25° (indicated by a dashed red line in Fig. 2) which can be identified with the carbon phase. The peak close to 38° and also minor peaks at 44°, 65°, and 78° can be identified with the gold (fcc) phase. The highest peak intensities was observed for the SC/AuNPs-C catalyst with the largest AuNPs size, and also shows the clearest features from the Au phase. On the other hand, the diffractograms of SC/AuNPs-A and SC/AuNPs-B were very similar. The differences in AuNPs sizes in the catalysts would likely have contributed to the differences in gold diffraction.

The surface morphology of the pristine SC, SC/AuNPs-A, SC/AuNPs-B and AuNPs-C catalysts was studied using SEM. It was observed that the morphological feature of the pristine SC (Fig. S1a) did not change after gold deposition (Fig. S1 b-d). Table 1 shows the specific surface areas (in m^2/g) and pore volumes (in cm^3/g) of the pristine SC and SC/AuNPs catalysts obtained from N_2 physisorption. Results show a general decrease in surface area and pore volume of the pristine SC upon deposition of AuNPs (Table 1). This is largely due to surface coverage with AuNPs and partial blockage of pores on the carbon support.

The electrochemically active surface area (ECSA) determined from the charge of Au oxide reduction for the three SC/AuNPs catalysts are also listed in Table 1. Also listed in Table 1 is the specific area of Au metal in each of the SC/AuNPs catalyst, calculated from the Au particle sizes obtained from TEM (see calculation in Table S2 of supporting information). Compared to the specific area of gold, the ECSA of the SC/AuNPs were relatively higher. This may be due to the contribution of capacitive current to the reduction charge of AuO (as seen in Fig. S2) which is inherent to the method used for ECSA determination.

3.2. ECH of glucose and xylose on mesoporous carbon-supported Au nanocatalysts

The ECH of glucose and xylose were tested using the prepared SC/AuNPs catalysts. Fig. 3 shows the linear sweep voltammograms recorded in 0.1 mol L^{-1} glucose (Fig. 3a) and in 0.1 mol L^{-1} xylose (Fig. 3b). The current densities were normalized to the ECSA of each catalyst. In both sugar solutions, all three SC/AuNPs catalysts showed a gradual increase in cathodic current from -1.1 V. However, towards more negative

Table 1
Au content, Au nanoparticle size, surface area and pore volume of mesoporous carbon-supported Au nanocatalysts.

Sample	Au loading (wt %)	Au average size (nm)	Au dispersion (%)	N_2 Physisorption Specific surface area (m^2/g)	Pore volume (cm^3/g)	ECSA (m^2/g)	Specific area of Au metal based on TEM (m^2/g)
SC/AuNPs-A	0.08 ± 0.01	4.4 ± 0.8	26.6	225	0.50	3.8	0.06
SC/AuNPs-B	0.19 ± 0.03	5.9 ± 1.4	19.8	213	0.48	4.9	0.10
SC/AuNPs-C	0.27 ± 0.03	10 ~ 30*	1.3	239	0.52	3.7	0.01
Pristine SC	–	–	–	309	0.61	–	–

* Aggregation of AuNPs was observed (see Fig. S6)

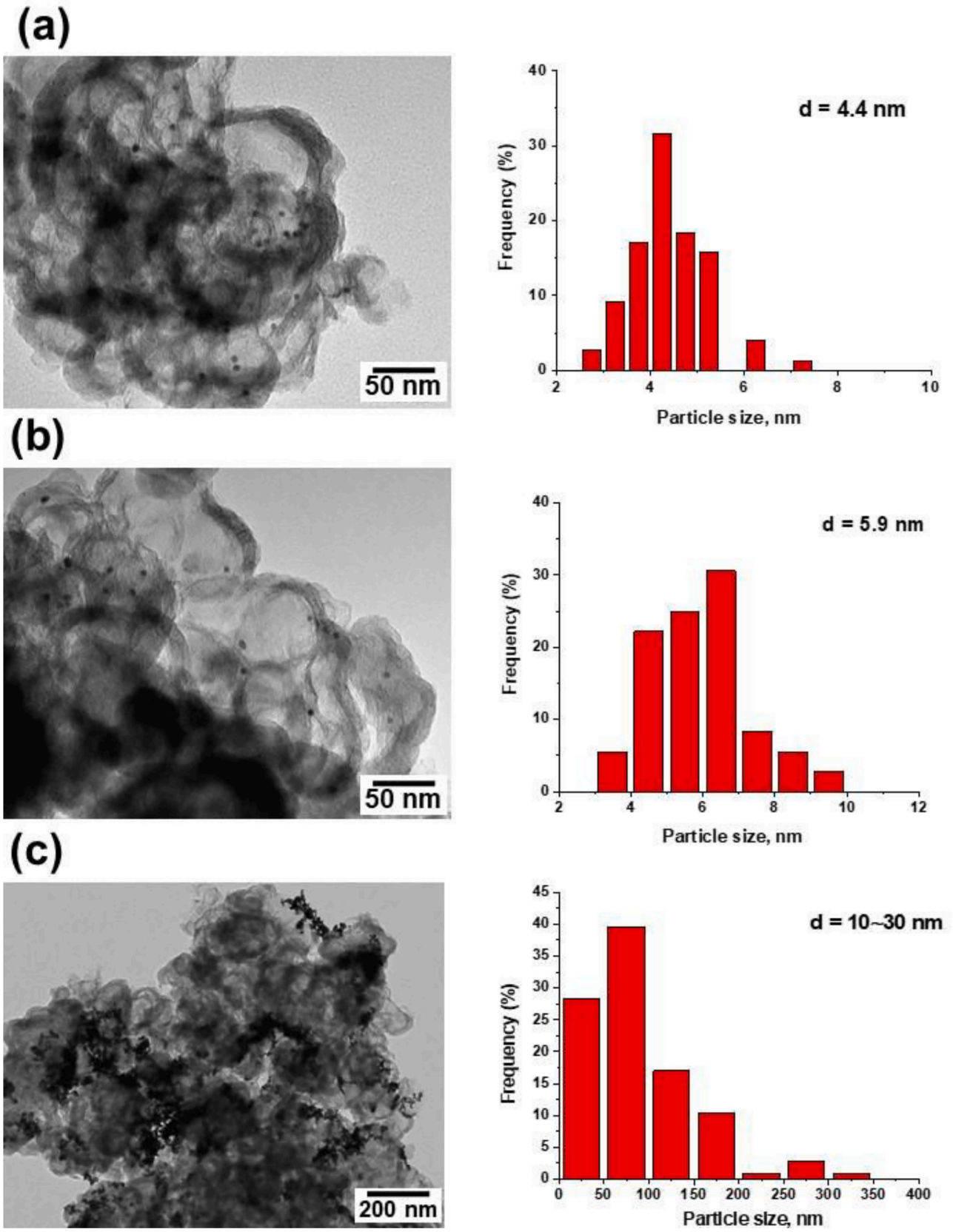

Fig. 1. TEM images and AuNPs particle size distribution of SC/AuNPs-A (a), SC/AuNPs-B (b), and SC/AuNPs-C (c).

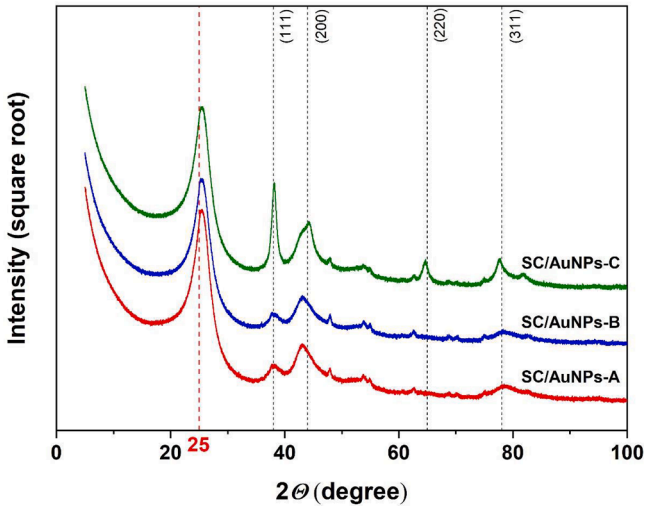

Fig. 2. X-ray diffraction patterns of SC/AuNPs-A, SC/AuNPs-B, and SC/AuNPs-C.

potentials starting from ca. -1.3 V in 0.1 mol L^{-1} glucose and from ca. –1.2 V in 0.1 mol L^{-1} xylose, SC/AuNPs-A catalyst yielded the highest currents followed by SC/AuNPs-B then SC/AuNPs-C. A higher cathodic current would indicate higher HER activity, which occurs concurrently with the ECH of glucose or xylose. Furthermore, the cathodic current recorded for the SC/AuNPs in xylose solution (Fig. 3b) were relatively higher compared to those recorded in glucose solution (Fig. 3a). This may be related to the extent of sugar adsorption on the catalyst surface that would inhibit HER activity

To further investigate the ECH of glucose and xylose, constant potential electrolyses at three different potentials (-1.0 V, -1.3 V, and -1.5 V) were carried out using the prepared SC/AuNPs catalysts in 0.1 mol L^{-1} glucose or xylose with 0.1 mol L^{-1} Na_2SO_4 as supporting electrolyte. ECH of glucose and xylose carried out on the mesoporous carbon support in the absence of AuNPs resulted in negligible yield of either sorbitol or xylitol (black line plots in Figs. 4b and 5b). Fig. 4 shows the turnover frequency (TOF) of glucose for each SC/AuNPs catalyst at different applied potentials (Fig. 4a) and the corresponding *FE*s (Fig. 4b) towards sorbitol formation. Reproducibility data of TOF (sorbitol, min^{-1}) for the different types of SC/AuNPs can be found in Table S4. Generally, the rate of glucose hydrogenation increased for each type of SC/AuNPs as the applied potential became more negative. At -1.5 V where the rate was highest, the TOF for sorbitol formation over SC/AuNPs-A, SC/AuNPs-B, and SC/AuNPs-C were 153 min^{-1}, 59 min^{-1}, and 40 min^{-1}, respectively. These results highlight the effect of Au cluster size on the hydrogenation rate, which was also observed when ECH was performed at -1.0 V and -1.3 V (Fig. 4a). The *FE* towards sorbitol formation also increased for all SC/AuNPs towards more negative potentials. At -1.5 V, the highest FE was recorded for SC/AuNPs-A (9.1 %) followed by SC/AuNPs-B (7.7 %) and SC/AuNPs-C (7.0 %). The upward trend in FE towards more negative potentials would likely be due to the higher extent of HER occurring on the surface of the negatively charged metal surface, thereby producing more adsorbed hydrogen available for sugar hydrogenation. Furthermore, HER produces hydroxide ions (Eqs. (1) and (4)) which increases the surface alkalinity of the metal that induces the mutarotation of cyclic glucose molecules into the electroactive linear form. As seen from the linear sweep voltammograms in glucose solution, HER is more extensive on SC/AuNPs-A and SC/AuNPs-B than on SC/AuNPs-C, which correlated with rates of glucose hydrogenation.

Fig. 5 shows the TOF (Fig. 5a) of xylose conversion into xylitol and the corresponding FE (Fig. 5b) over the prepared SC/AuNPs catalysts. Similar to the glucose hydrogenation, the TOF increased for each type of SC/AuNPs catalyst as the applied potential became more negative. At -1.5 V, the recorded TOFs were 55, 34, 20 min^{-1} for SC/AuNPs-A, SC/AuNPs-B, and SC/AuNPs-C, respectively. The effect of Au cluster size on the xylose ECH rate was also observed at all applied potentials (Fig. 5a), wherein higher activity is associated with smaller particle size. However, the metal cluster size effect was at a less extent as that observed in glucose ECH. The FE on the other hand, followed a downward trend towards more negative potentials unlike that observed for the hydrogenation of glucose, with highest FEs recorded at -1.0 V. At -1.0 V, the SC/AuNPs-C recorded the highest FE (14.2 %) followed by SC/AuNPs-B (12.9 %) then SC/AuNPs-A (6.9 %). Differences in FE values among the three catalysts became smaller towards more negative potentials.

3.3. *In-situ FTIR-ATR spectroscopy*

Relating to the differences in *FE*s between glucose and xylose ECH as a function of applied potential, *in-situ* FTIR-ATR spectroscopy was performed to observe the reactions occurring at catalyst surface during glucose and xylose ECH. The spectra were recorded at different potentials from 0 V to -1.3 V vs Ag/AgCl applied to a sputtered Au electrode in 0.1 mol L^{-1} Na_2SO_4 containing 0.1 M glucose or xylose solution. Fig. 6 shows the spectra recorded in 0.1 mol L^{-1} glucose (Fig. 6a) and in 0.1 mol L^{-1} xylose (Fig. 6b) during ECH with the spectrum recorded at 0 V taken as the reference spectrum. The corresponding spectral

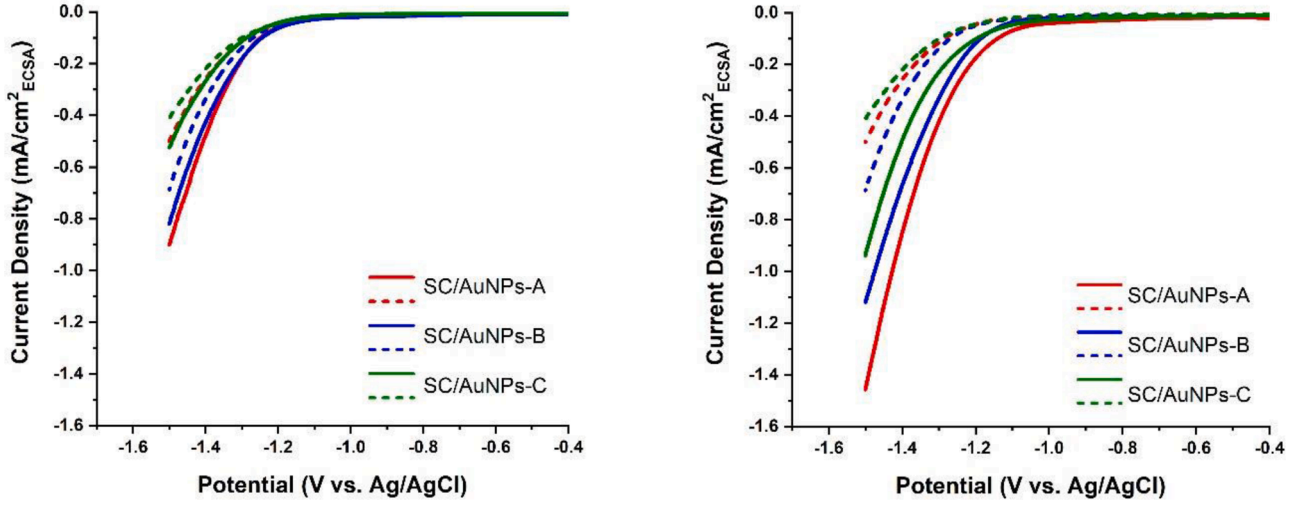

Fig. 3. Linear sweep voltammograms of SC/AuNPs-A, SC/AuNPs-B, and SC/AuNPs-C in 0.1 mol L^{-1} glucose (a) and in 0.1 mol L^{-1} xylose (b) with 0.1 mol L^{-1} Na_2SO_4 electrolyte. The dashed lines in both Fig.s correspond to the voltammograms recorded in the supporting electrolyte only. The scan rate is 5 mV s^{-1}.

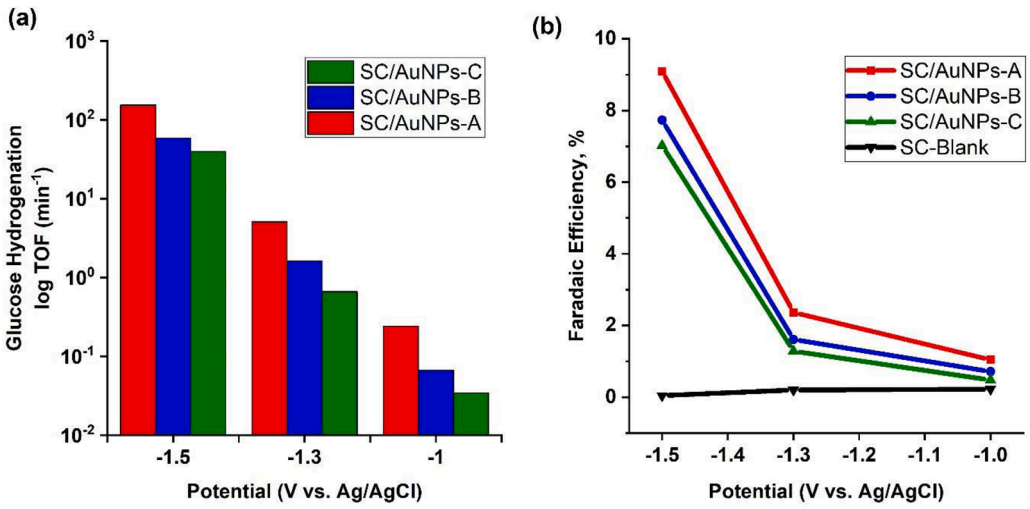

Fig. 4. ECH rates of glucose to sorbitol over the SC/AuNPs catalysts at different applied potentials (a) and FE of sorbitol recorded at each applied potential. ECH of glucose was performed in 0.1 mol L^{-1} Na_2SO_4 (initial pH ≈ 7) as background electrolyte and at room temperature and pressure with stirring speed of 300 rpm.

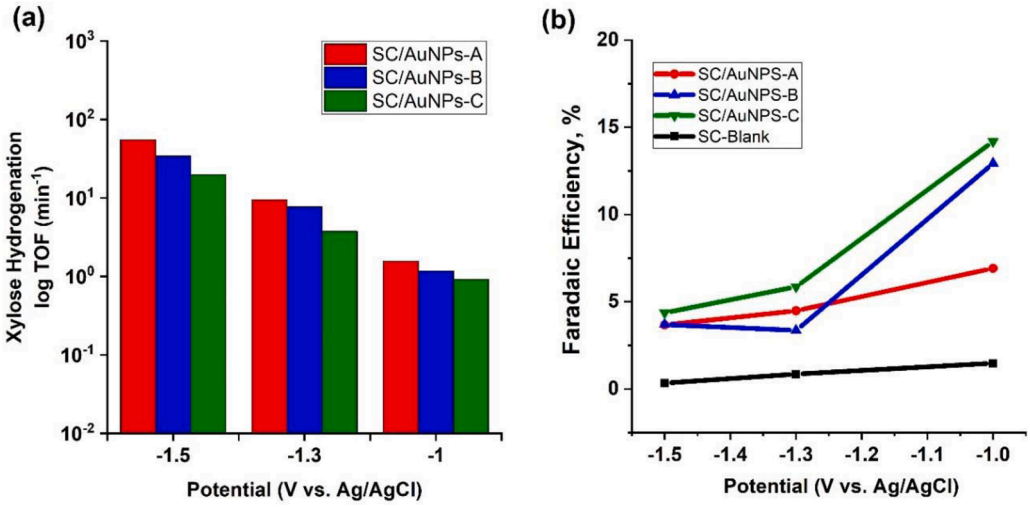

Fig. 5. ECH rates of xylose to xylitol over the SC/AuNPs catalysts at different applied potentials (a) and FE of xylitol recorded at each applied potential. ECH of xylose was performed in 0.1 mol L^{-1} Na_2SO_4 (initial pH ≈ 7) as background electrolyte and at room temperature and pressure with stirring speed of 300 rpm.

assignments are listed in Table S3. The formation of the sugar alcohol product is indicated by the bands at ca. 810 and 1110 cm^{-1}, which appear from -0.7 V until -1.3 V in both glucose (S3a) and xylose (S3b) solutions. Both of these bands correspond to the C-C-O stretching in primary alcohols. The shoulder at ca. 1750 cm^{-1} seen in both glucose and xylose solutions in Fig. 6 corresponds to the C=O stretching vibrations from the open aldehyde form of glucose and xylose. The band at ca. 1650 cm^{-1} found in both glucose and xylose solutions (Fig. 6) would correspond to the 1,2-enediol intermediate as observed in the work by Yaylayan et al. [51] in aqueous sugar solutions. In acidic or basic environment, sugars can undergo Lobry de Bruyn-van Ekenstein transformation that converts the aldose into the ketose isomer of the sugar via the enediol intermediate [52]. As the applied potentials become more negative, the electrocatalytic water-splitting becomes more extensive which increases the surface alkalinity. A more alkaline environment would in turn, promote the enolization of glucose or xylose as indicated by the increase in intensity of the absorption band around 1650 cm^{-1} towards more negative potentials. The spectra in both glucose and xylose solutions in Fig. 6 also show a strong band at ca. 2345 cm^{-1}, which corresponds to the asymmetric stretch (O=C=O) of interfacial CO_2 [53,54].

As observed in both glucose and xylose solutions, the IR band at ca. 3500 cm^{-1} increases from -0.7 V (Fig. S3) and is assigned to the OH stretching vibration of water molecules on the surface of the electrode [55]. This absorption band is more intense in glucose solution than in xylose solution at -1.0 V as shown in Fig. 7a, which indicates that water adsorption is more extensive in glucose solution at this potential. Conversely, at -1.3 V (Fig. 7b) the absorbance at 3500 cm^{-1} was lower in glucose solution than in xylose solution, indicating higher adsorption of water in the latter. Assuming that water adsorption is the precursor for HER, the data suggests that the extent of HER is higher in glucose at -1.0 V than in xylose. HER activity increases gradually in xylose solution from -1.0 to -1.3 V as indicated by the increasing absorbance at 3500 cm^{-1} as shown in Fig. S4b. The increase in absorbance intensity was relatively lower in glucose solution (Fig. S4a). Considering that HER is the major competing reaction, this would explain the downward trend in *FE* for xylitol formation towards more negative potentials. At -1.3 V, HER becomes more active in xylose solution than in glucose as evidenced by the absorbance at 3500 cm^{-1} at this potential (Fig. 7b). This is further supported by the LSV data shown in Fig. 3, where the cathodic currents are higher in xylose solution than in glucose at -1.3 V.

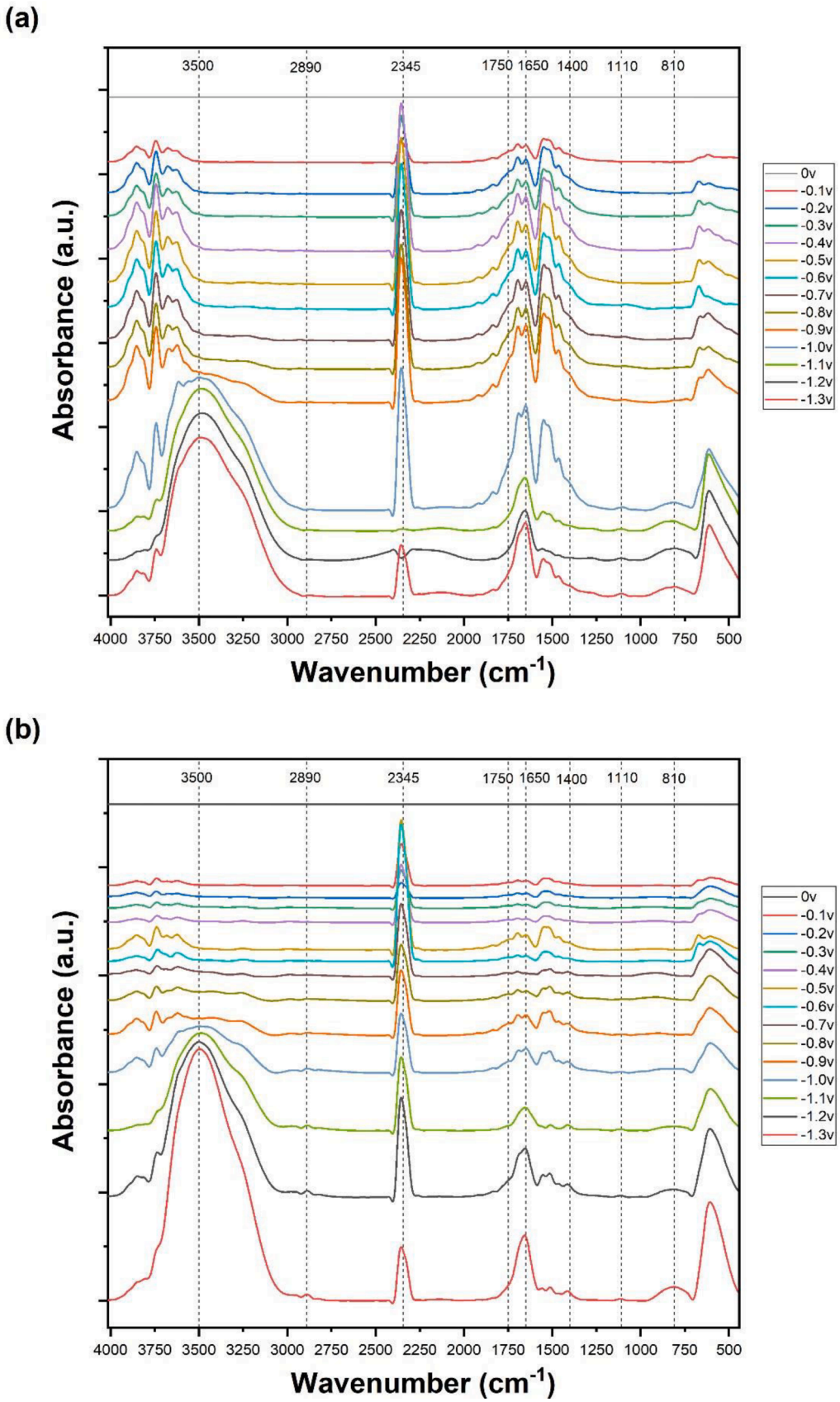

Fig. 6. In situ FTIR-ATR spectra recorded at various potentials on a sputtered Au electrode in 0.1 M Na_2SO_4 containing 0.1 M glucose (a) and 0.1 M xylose (b). The reference spectrum was the spectrum recorded at 0 V for each of the sugar solutions.

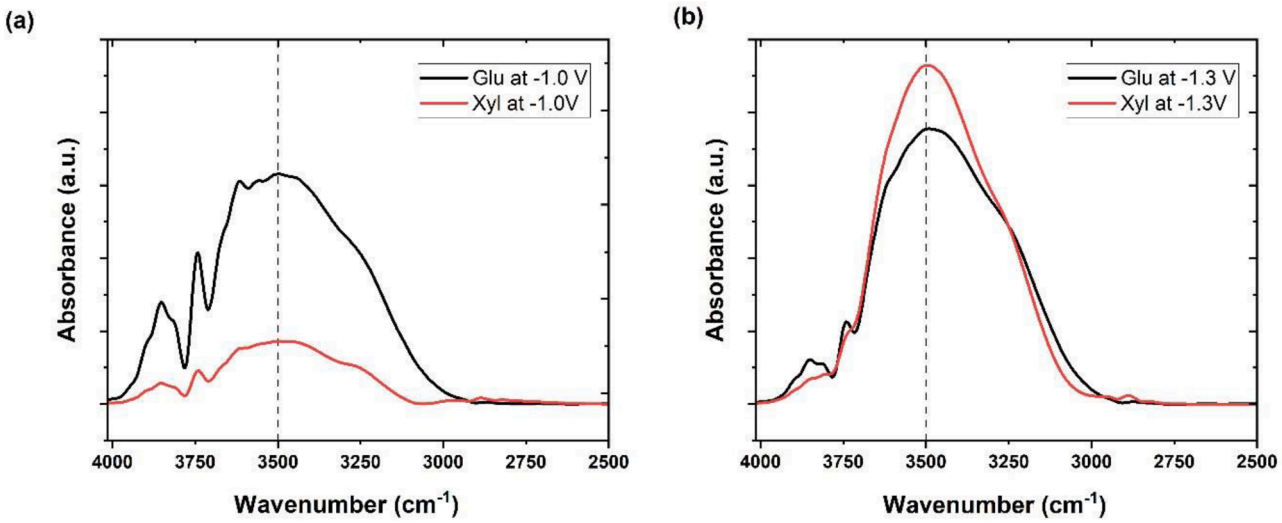

Fig. 7. In situ FTIR-ATR spectra recorded in 0.1 mol L^{-1} glucose and 0.1 mol L^{-1} xylose at -1.0 V (a) and -1.3 V (b) with 0.1 mol L^{-1} Na_2SO_4 as background electrolyte. The reference spectrum was the spectrum recorded at 0 V for each of the sugar solutions.

3.4. Long-term ECH of glucose and xylose on the SC/AuNPs-A catalyst

Fig. 8 shows the conversion rates and corresponding FE for glucose (Fig. 8a) and xylose (Fig. 8b) on the SC/AuNPs-A catalyst at the potential range from -1.0 V to -1.6 V. The conversion rate reached a maximum at -1.5 V for both glucose and xylose ECH. Prolonged electrolysis was carried out at this potential in both glucose and xylose solutions. Fig. 9 shows the concentrations of sorbitol (Fig. 9a) and xylitol (Fig. 9b) through time and their corresponding *FE*.

As shown in Fig. 9, there was a general decrease in *FE* for both sorbitol (Fig. 9a) and xylitol (Fig. 9b) within the first hour of electrolysis. This was largely due to the active HER characterized by continuous bubbling on the working electrode. The extensive bubbling caused the catalyst particles to be pushed out of the carbon felt support, as observed with the darkening of the reaction solution as the electrolyses progressed. Therefore, an improvement in the working electrode configuration is warranted. At the end of the 6 hour electrolysis experiments, the concentrations of sorbitol and xylitol were 3.0 mmol L^{-1} and 1.9 mmol L^{-1}, respectively. These correspond to a sorbitol yield of 2.5% and a xylitol of 1.3%, both with *FE* of 1.2 %. This is an improvement from our earlier work on sugar ECH over microporous carbon-supported AuNPs with wider cluster size distributions [42]. Higher *FE* for sorbitol can be obtained over RaNi catalyst (40-67%) [29,56] and metals with higher HER overpotential such as Pb(Hg) (15 %) [31], Zn (21 %) [31], and Zn (Hg) (16-39 %) [29,32]. Kwon et al. also observed a high selectivity towards sorbitol (87%) over a Pb catalyst during ECH of glucose in an undivided cell at a high overpotential (-1.83 vs RHE) [33]. On the other hand, Jokic et al. [34] reported high FE for xylitol (> 80 %) from xylose ECH using Zn(Hg) catalyst. Using an Zn-Fe electrocatalyst deposited on a carbon nanotube (CNT) support, Fei et al. carried out ECH of glucose with sorbitol *FE* of 57% [57]. Recently, Liang et al. [58] studied the electrochemical reduction of the simple monosaccharides – dihydroxyacetone (DHA) and glyceraldehyde (GA), on palladium metal. *FE*s of 31-35 % were obtained towards the main reduction products (acetol from DHA and 3-hydroxypropionaldehyde from GA) under optimum potential and pH conditions. Although the values obtained in this work are considerably lower, the study demonstrated that the yield and *FE* of glucose and xylose ECH can be improved by controlling the applied potential and the metal cluster size of supported metal catalyst.

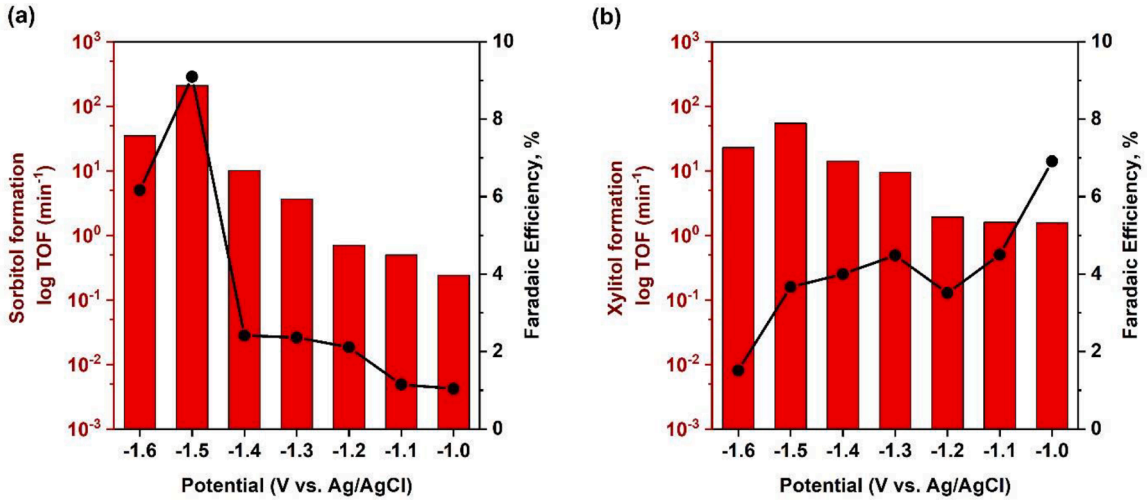

Fig. 8. Variation of TOF and FE for glucose (a) and xylose (b) on the SC/AuNPs-A catalyst at the potential range of -1.0 V to -1.6 V (vs Ag/AgCl). ECH of glucose or xylose was performed in 0.1 mol L^{-1} Na_2SO_4 (initial pH ≈ 7) as background electrolyte and at room temperature and pressure with stirring speed of 300 rpm.

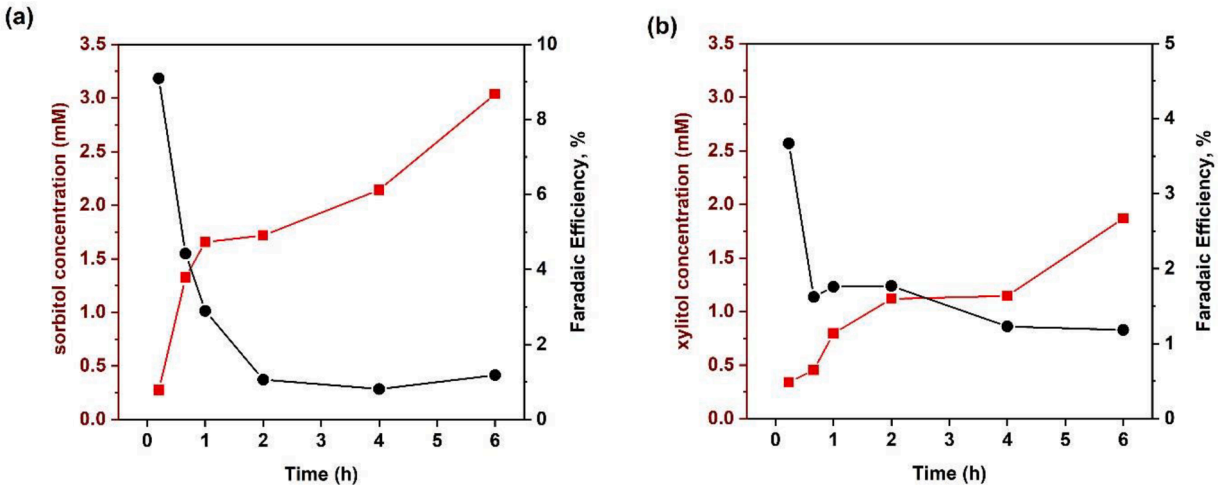

Fig. 9. Plot of the concentration and FE for sorbitol (a) and xylitol (b) on the SC/AuNPs-A catalyst over time at an applied potential of -1.5 V (vs Ag/AgCl). Constant-potential electrolysis of glucose or xylose was performed in 0.1 mol L^{-1} Na_2SO_4 (initial pH ≈ 7) as background electrolyte and at room temperature and pressure with stirring speed of 300 rpm.

3.5. ECO of glucose and xylose on mesoporous carbon-supported Au nanocatalysts

The ECO of glucose and xylose were carried out using the same set of SC/AuNPs catalysts. Fig. S5 shows the cyclic voltammograms of the SC/AuNPs catalysts recorded in the background electrolyte (0.1 mol L^{-1} NaOH). The peak around -0.1 V would correspond to the adsorption of OH^- ions with a corresponding desorption peak at ca. -0.2 V in backward scan. The oxidation of Au starts at ca. +0.2 V and also evident with the shoulder around +0.5 V. An oxidation peak was also observed at ca. +0.2 V in the backward scan for all the SC/AuNPs. This could be attributed to the adsorption of OH^- on the surface of the reduced Au oxide or removal of blocking species on the surface of the catalyst [59]. Fig. 10 shows the cyclic voltammograms recorded for the three SC/AuNPs catalysts in 0.1 mol L^{-1} NaOH containing 0.1 mol L^{-1} glucose and 0.1 mol L^{-1} xylose. In the forward scan, an oxidation peak at ca. +0.3 V with a shoulder at ca. -0.05 V was observed with the SC/AuNPs-A and SC/AuNPs-C catalysts in both glucose (Fig. 10a) and xylose (Fig. 10b) solutions. These correspond to the oxidation of glucose or xylose on Au sites with adsorbed OH- ions. For the SC/AuNPs-B catalyst, the main oxidation peak for glucose (Fig. 10a) or xylose (Fig. 10b) occurs at slightly more positive potential at ca. +0.4 V with a shoulder also at ca. -0.05 V. In the reverse scan, a broad oxidation peak was observed in all of the three SC/AuNPs catalysts at around +0.4 V in both glucose and xylose solutions. This would correspond to the oxidation of either glucose or xylose on the fresh Au surface as Au oxide is being reduced. This phenomenon was also observed in the works of Holade et al. [12] and Sugano et al. [59] on the electro-oxidation of glucose and cellulose, respectively, on gold catalyst. Towards more negative potentials, a reduction peak at ca. -0.2 V was observed in all catalysts, which corresponds to the desorption of OH^- ions.

Taking into account the different potentials at which glucose or xylose oxidation may occur, electrolysis experiments were carried out at -0.05 V, +0.3 V, and +0.4 V. Fig. 11 shows the TOFs for gluconic acid and xylonic acid on the SC/AuNPs catalysts after a three-hour electrolysis at different potentials. In both glucose and xylose electro-oxidation, the effect of Au cluster size on the TOF was observed at all applied potentials. Representative data for TOF reproducibility for glucose ECO (at +0.4 V) over the different types of SC/AuNPs catalysts are listed in Table S5. For the glucose ECO (Fig. 11a), the highest TOFs were recorded for SC/AuNPs-A at -0.05 V, +0.3 V, and +0.4 V with rates of 77 min^{-1}, 300 min^{-1}, and 197 min^{-1}, respectively. SC/AuNPs-B had the highest TOF (33 min^{-1}) at +0.4 V, while for SC/AuNPs-C TOF was highest at +0.3 V (65 min^{-1}). For the xylose ECO, SC/AuNPs-A also had

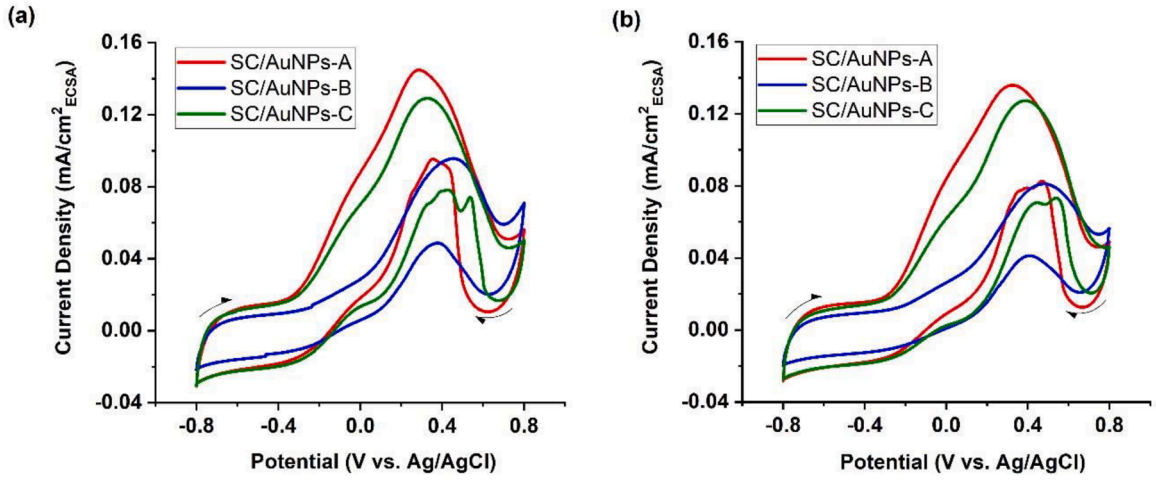

Fig. 10. Cyclic voltammograms recorded for SC/AuNPs-A (red line), SC/AuNPs-B (blue line), and SC/AuNPs-C (green line) in N_2-purged solution of 0.1 M NaOH with 0.1 M glucose (a) and 0.1 M xylose (b). The scan rate was 10 mV s^{-1}.

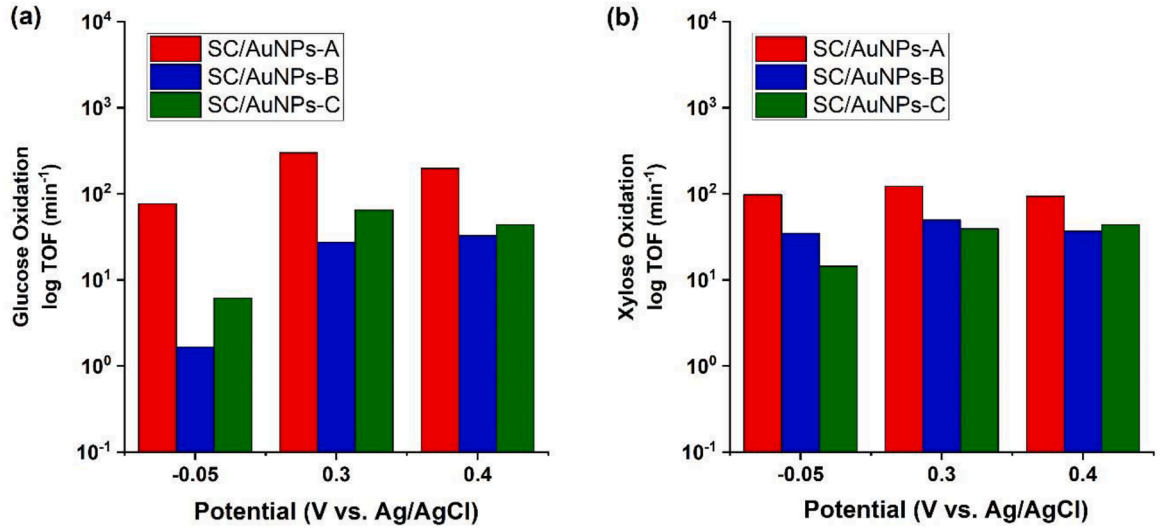

Fig. 11. ECO rates of glucose (a) and xylose (b) over the different SC/AuNPs catalysts at various applied potentials. ECO of glucose or xylose was performed in 0.1 M NaOH as background electrolyte and at room temperature and pressure with stirring speed of 300 rpm. FE was close to 100% for all the electrolyses carried out.

the highest TOF among the three catalysts at all the applied potentials (Fig. 11b). The oxidation rates of xylose over SC/AuNPs-A at -0.05 V, +0.3 V, and +0.4 V were 98 min^{-1}, 122 min^{-1}, and 93 min^{-1}, respectively. The rate was highest for SC/AuNPs-B (50 min^{-1}) at +0.3 V while for SC/AuNPs-C, TOF was highest at +0.4 V (44 min^{-1}). For all the SC/AuNPs catalysts studied, the sugar acid (gluconic acid or xylonic acid) was the major product, with *FEs* close to 100%. Major side products formed were fructose and xylulose, produced from the base-catalyzed isomerization of glucose and xylose, respectively, in the bulk solution.

As the highest glucose and xylose ECO rates were observed with SC/AuNPs-A, long-term electrolysis was done using this catalyst to observe the product formation as a function of time. Constant-potential electrolysis was carried out at +0.3 V in glucose and xylose solutions for 6 h and the reaction products were analysed using HPLC. Fig. 12 shows the amount of gluconic acid (Fig. 12a) and xylonic acid (Fig. 12b) produced at various points during glucose and xylose ECO, respectively. Steady state was achieved for glucose ECO after 3 h of reaction while that for xylose ECO was achieved after 4 h. The decrease in conversion rate is likely due to the depletion of hydroxide ions, as indicated by the gradual decrease in pH of the reaction solutions during the progress of electrolysis. The FE was close to 100% throughout the glucose or xylose ECO, and was calculated based on a two-electron oxidation process for both sugars. At the end of the 6-hour electrolysis experiments, 65 mmol L^{-1} of gluconic acid and 48 mmol L^{-1} of xylonic acid were produced corresponding to 42 % and 32 % conversion, respectively. Higher glucose and xylose conversions (67 and 52 %, respectively) were obtained by Rafaïdeen et al. for sugar electro-oxidation over Pd_3Au_7/C with higher metal loading (41.3 wt. %) [9]. On bare Au anode, Moggia and co-workers obtained a glucose conversion of 25 % with 97.6 % selectivity after 6 h of experiment (0.04 M glucose concentration, pH of 11.3, 5 °C, +0.6 V vs. RHE) [60]. Electro-oxidation of xylose over an Au electrode at 1.1 V (vs RHE) for 6 h resulted in a xylose conversion of 98 % with a selectivity of 63 % to xylonic acid [61]. For comparison, heterogeneous catalytic oxidation of glucose on Au/C catalyst has been shown to yield 90% of gluconic acid under base-free conditions (0.1 MPa O_2 and 40 °C) [62]. An earlier study on glucose oxidation over 1% Au/C catalyst at pH 9.5 displayed high activity (TOF = 500 h^{-1}) and selectivity (99 %) towards gluconate formation [63]. Other studies on glucose oxidation show the dependence of conversion rate on the alkalinity of the reaction solution [64] and the Au particle size [65]. Thermal catalytic oxidation of xylose over Au catalysts at 100-130 °C provide high yields of xylonic acid (83-98 %) [66,67] as has also been

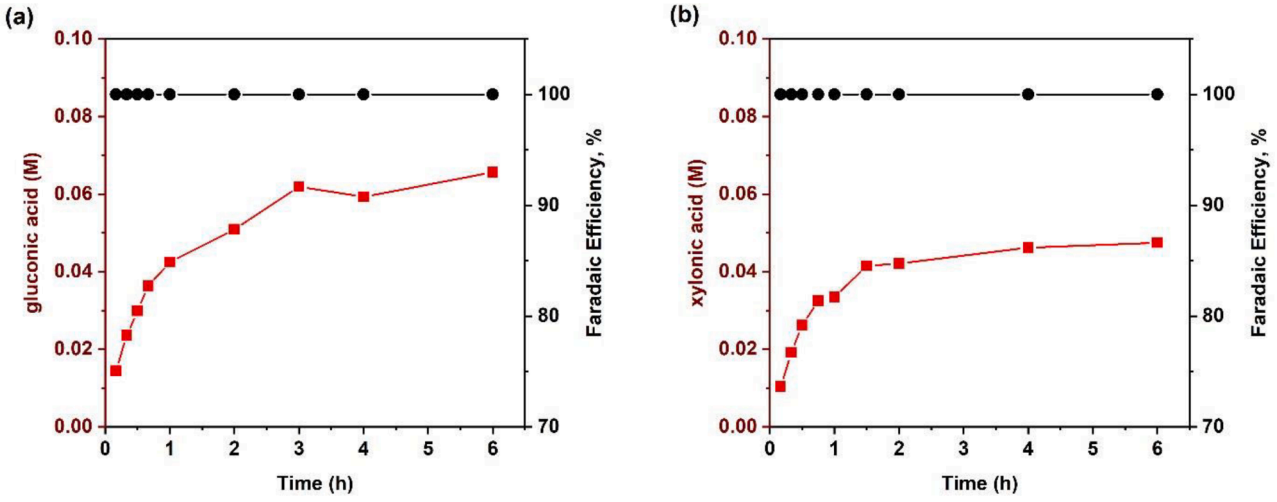

Fig. 12. Plot of the concentration of gluconic acid (a) and xylonic acid (b) produced over time on the SC/AuNPs-A catalysts and corresponding FEs. ECO of glucose or xylose was performed in 0.1 M NaOH as background electrolyte at +0.3 V (vs Ag/AgCl) for 6 hours at room temperature and pressure with stirring speed of 300 rpm.

observed for photocatalytic oxidation over Au/TiO_2 (96-98 %) [68].

Major side products formed were fructose and xylulose, as observed in the screening experiments. Furthermore, aggregation of AuNPs was observed as evidenced by the larger average AuNPs sizes of the spent catalysts from TEM analysis (Fig. S7) compared to the pristine catalyst (Fig. 1.)

4. Conclusion

Electrocatalytic hydrogenation and oxidation of glucose and xylose were accomplished over mesoporous carbon (Sibunit)-supported gold nanoparticles (AuNPs). AuNPs were deposited on the mesoporous carbon from prepared gold sols with different average Au cluster sizes. Size control of AuNPs was achieved by varying the concentration of the gold precursor ($HAuCl_4$). The fabricated SC/AuNPs catalysts were then characterized by physico-chemical and electrochemical methods. The activity of the SC/AuNPs catalysts towards sugar electro-hydrogenation (ECH) and electro-oxidation (ECO) was tested using constant potential electrolysis.

For glucose and xylose ECH, the hydrogenation rate increased towards more negative applied potentials until -1.5 V. This would indicate that ECH rate depends on the extent of HER which involves chemisorbed hydrogen atoms on the surface of the Au catalyst. The influence of AuNPs size on the hydrogenation rate was more evident in glucose ECH than that for xylose, wherein smaller AuNPs were observed to be more active. In glucose ECH, the reaction rate and selectivity (*FE*) increased towards more negative applied potentials. The rate also increased in xylose ECH as the applied potentials became more negative but the *FE* followed an opposite trend. Analysis using *in-situ* ATR-FTIR spectroscopy showed that water adsorption (and therefore HER), was more extensive in xylose solution than in glucose at more negative potentials. This may have inhibited xylose ECH to a greater extent than glucose ECH. Prolonged electrolysis using the most active catalyst (SC/AuNPs-A) in glucose and xylose solutions at -1.5 V resulted in low yields for sorbitol or xylitol mainly due to the mechanical detachment of the SC/AuNPs catalyst powder from the carbon felt holder under vigorous HER. Therefore, a better catalyst configuration for these reactions is necessary.

The same set of catalysts were investigated for the electro-oxidation of glucose and xylose. From cyclic voltammetry measurements, the sugar ECO occurred at -0.05 V, +0.3 V, and +0.4 V using the electrocatalytic set-up in this work. SC/AuNPs-A, with the smallest AuNPs, were more active towards glucose or xylose ECO than SC/AuNPs-B and SC/AuNPs-C at all the applied potentials. These results indicate preference for smaller Au cluster size for sugar ECO. At the end of a 6 h electrolysis, a 42 % and 32 % conversion for gluconic acid and xylonic acid, respectively, was obtained.

CRediT authorship contribution statement

Jay Pee Oña: Investigation, Data curation, Writing – original draft. **Rose-Marie Latonen:** Methodology, Investigation, Writing – review & editing, Supervision. **Narendra Kumar:** Methodology, Investigation, Writing – review & editing. **Markus Peurla:** Investigation. **Ilari Angervo:** Investigation. **Henrik Grénman:** Conceptualization, Methodology, Writing – review & editing, Supervision, Data curation, Funding acquisition.

Declaration of Competing Interest

The authors declare that they have no known competing financial interests or personal relationships that could have appeared to influence the work reported in this paper.

Data availability

Data will be made available on request.

Acknowledgements

This research is part of the FosToBioH2 (From fossil to biohydrogen in Finnish (bio)industry - utilizing electrocatalysis in Aqueous Phase Reforming of hemicelluloses) project at Åbo Akademi University, Finland. The authors would like to thank the Tiina and Antti Herlin Foundation (Finland) for their significant financial support. We also thank the Electron Microscopy Laboratory, Institute of Biomedicine, University of Turku, and Biocenter Finland for the TEM images, the Wihuri Physical Laboratory, Department of Physics and Astronomy, University of Turku for the XRD analysis and L. Silvander (Åbo Akademi University) for the SEM analysis.

Supplementary materials

Supplementary material associated with this article can be found, in the online version, at doi:10.1016/j.electacta.2022.141536.

References

[1] F.W.S. Lucas, R.G. Grim, S.A. Tacey, C.A. Downes, J. Hasse, A.M. Roman, C. A. Farberow, J.A. Schaidle, A. Holewinski, Electrochemical routes for the valorization of biomass-derived feedstocks: from chemistry to application, ACS Energy Lett. 6 (2021), https://doi.org/10.1021/acsenergylett.0c02692.

[2] S.A. Akhade, N. Singh, O.Y. Gutierrez, J. Lopez-Ruiz, H. Wang, J.D. Holladay, Y. Liu, A. Karkamkar, R.S. Weber, A.B. Padmaperuma, M.S. Lee, G.A. Whyatt, M. Elliott, J.E. Holladay, J.L. Male, J.A. Lercher, R. Rousseau, V.A. Glezakou, Electrocatalytic hydrogenation of biomass-derived organics: a review, Chem. Rev. 120 (2020), https://doi.org/10.1021/acs.chemrev.0c00158.

[3] C.H. Lam, W. Deng, L. Lang, X. Jin, X. Hu, Y. Wang, Minireview on bio-oil upgrading via electrocatalytic hydrogenation: connecting biofuel production with renewable power, Energy Fuels 34 (2020), https://doi.org/10.1021/acs.energyfuels.0c01380.

[4] Y.P. Wijaya, K.J. Smith, C.S. Kim, E.L. Gyenge, Electrocatalytic hydrogenation and depolymerization pathways for lignin valorization: toward mild synthesis of chemicals and fuels from biomass, Green Chem. 22 (2020), https://doi.org/10.1039/d0gc02782k.

[5] L. Zhang, T.U. Rao, J. Wang, D. Ren, S. Sirisommboonchai, C. Choi, H. Machida, Z. Huo, K. Norinaga, A review of thermal catalytic and electrochemical hydrogenation approaches for converting biomass-derived compounds to high-value chemicals and fuels, Fuel Process. Technol. 226 (2022), https://doi.org/10.1016/j.fuproc.2021.107097.

[6] M. Simões, S. Baranton, C. Coutanceau, Electrochemical valorisation of glycerol, ChemSusChem 5 (2012), https://doi.org/10.1002/cssc.201200335.

[7] Y. Kwon, K.J.P. Schouten, M.T.M. Koper, Mechanism of the catalytic oxidation of glycerol on polycrystalline gold and platinum electrodes, ChemCatChem 3 (2011), https://doi.org/10.1002/cctc.201100023.

[8] C. Dai, L. Sun, H. Liao, B. Khezri, R.D. Webster, A.C. Fisher, Z.J. Xu, Electrochemical production of lactic acid from glycerol oxidation catalyzed by AuPt nanoparticles, J. Catal. 356 (2017), https://doi.org/10.1016/j.jcat.2017.10.010.

[9] T. Rafaïdeen, S. Baranton, C. Coutanceau, Highly efficient and selective electrooxidation of glucose and xylose in alkaline medium at carbon supported alloyed PdAu nanocatalysts, Appl. Catal. B 243 (2019), https://doi.org/10.1016/j.apcatb.2018.11.006.

[10] M. Pasta, F. la Mantia, Y. Cui, Mechanism of glucose electrochemical oxidation on gold surface, Electrochim. Acta 55 (2010), https://doi.org/10.1016/j.electacta.2010.04.069.

[11] G. Moggia, T. Kenis, N. Daems, T. Breugelmans, Electrochemical oxidation of d-glucose in alkaline medium: impact of oxidation potential and chemical side reactions on the selectivity to d-gluconic and d-glucaric acid, ChemElectroChem 7 (2020), https://doi.org/10.1002/celc.201901592.

[12] Y. Holade, K. Servat, T.W. Napporn, C. Morais, J.M. Berjeaud, K.B. Kokoh, Highly selective oxidation of carbohydrates in an efficient electrochemical energy converter: cogenerating organic electrosynthesis, ChemSusChem 9 (2016), https://doi.org/10.1002/cssc.201501593.

[13] M. Tominaga, T. Shimazoe, M. Nagashima, I. Taniguchi, Electrocatalytic oxidation of glucose at gold nanoparticle-modified carbon electrodes in alkaline and neutral solutions, Electrochem. Commun. 7 (2005), https://doi.org/10.1016/j.elecom.2004.12.006.

[14] M. Tominaga, T. Shimazoe, M. Nagashima, H. Kusuda, A. Kubo, Y. Kuwahara, I. Taniguchi, Electrocatalytic oxidation of glucose at gold-silver alloy, silver and

gold nanoparticles in an alkaline solution, J. Electroanal. Chem. 590 (2006), https://doi.org/10.1016/j.jelechem.2006.02.018.
[15] W.J. Liu, L. Dang, Z. Xu, H.Q. Yu, S. Jin, G.W. Huber, Electrochemical oxidation of 5-hydroxymethylfurfural with NiFe layered double hydroxide (LDH) nanosheet catalysts, ACS Catal 8 (2018), https://doi.org/10.1021/acscatal.8b01017.
[16] B. You, X. Liu, X. Liu, Y. Sun, Efficient H2 evolution coupled with oxidative refining of alcohols via a hierarchically porous nickel bifunctional electrocatalyst, ACS Catal. 7 (2017), https://doi.org/10.1021/acscatal.7b00876.
[17] B. You, X. Liu, N. Jiang, Y. Sun, A general strategy for decoupled hydrogen production from water splitting by integrating oxidative biomass valorization, J. Am. Chem. Soc. 138 (2016), https://doi.org/10.1021/jacs.6b07127.
[18] V.P. Kashparova, V.A. Klushin, D. v. Leontyeva, N. v. Smirnova, V.M. Chernyshev, V.P. Ananikov, Selective synthesis of 2,5-diformylfuran by sustainable 4-acetamido-tempo/halogen-mediated electrooxidation of 5-hydroxymethylfurfural, Chem. Asian J. 11 (2016), https://doi.org/10.1002/asia.201600801.
[19] S. Thiyagarajan, D. Franciolus, R.J.M. Bisselink, T.A. Ewing, C.G. Boeriu, J. van Haveren, Selective production of maleic acid from furfural via a cascade approach combining photochemistry and electro- or biochemistry, ACS Sustain. Chem. Eng. 8 (2020), https://doi.org/10.1021/acssuschemeng.0c02833.
[20] P. Parpot, A.P. Bettencourt, G. Chamoulaud, K.B. Kokoh, E.M. Belgsir, Electrochemical investigations of the oxidation-reduction of furfural in aqueous medium - Application to electrosynthesis, Electrochim. Acta (2004) 49, https://doi.org/10.1016/j.electacta.2003.08.021.
[21] P. Mäki-Arvela, B. Holmbom, T. Salmi, D.Y. Murzin, Recent progress in synthesis of fine and specialty chemicals from wood and other biomass by heterogeneous catalytic processes, Catal. Rev. Sci. Eng. 49 (2007), https://doi.org/10.1080/01614940701313127.
[22] M. Andérez Fernández, J. Rissanen, A. Pérez Nebreda, C. Xu, S. Willför, J. García Serna, T. Salmi, H. Grénman, Hemicelluloses from stone pine, holm oak, and Norway spruce with subcritical water extraction – comparative study with characterization and kinetics, J. Supercrit. Fluids 133 (2018), https://doi.org/10.1016/j.supflu.2017.07.001.
[23] F.M. Yedro, H. Grénman, J.v. Rissanen, T. Salmi, J. García-Serna, M.J. Cocero, Chemical composition and extraction kinetics of Holm oak (Quercus ilex) hemicelluloses using subcritical water, J. Supercrit. Fluids (2017) 129, https://doi.org/10.1016/j.supflu.2017.01.016.
[24] G. Gallina, Á. Cabeza, H. Grénman, P. Biasi, J. García-Serna, T. Salmi, Hemicellulose extraction by hot pressurized water pretreatment at 160 °C for 10 different woods: Yield and molecular weight, J. Supercrit. Fluids 133 (2018), https://doi.org/10.1016/j.supflu.2017.10.001.
[25] A.P. Nebreda, H. Grénman, P. Mäki-Arvela, K. Eränen, J. Hemming, S. Willför, D. Y. Murzin, T. Salmi, Acid hydrolysis of O-acetyl-galactoglucomannan in a continuous tube reactor: A new approach to sugar monomer production, Holzforschung (2016) 70, https://doi.org/10.1515/hf-2014-0314.
[26] X. Lu, P. Junghans, J. Wärnå, G. Hilpmann, R. Lange, H. Trajano, K. Eränen, L. Estel, S. Leveneur, H. Grénman, Hydrolysis of semi-industrial aqueous extracted xylan from birch (Betula pendula) employing commercial catalysts: kinetics and modelling, J. Chem. Technol. Biotechnol. (2022) 97, https://doi.org/10.1002/jctb.6918.
[27] X. Lu, P. Junghans, S. Weckesser, J. Wärnå, G. Hilpmann, R. Lange, H. Trajano, K. Eränen, L. Estel, S. Leveneur, H. Grénman, One flow through hydrolysis and hydrogenation of semi-industrial xylan from birch (betula pendula) in a continuous reactor—Kinetics and modelling, Chem. Eng. Process. Process Intensification (2021) 169, https://doi.org/10.1016/j.cep.2021.108614.
[28] T. Werpy, G. Petersen, Top value added chemicals from biomass, U.S, Department of Energy 1 (2004), https://doi.org/10.2172/926125.
[29] K. Park, P.N. Pintauro, M.M. Baizer, K. Nobe, Flow reactor studies of the paired electro-oxidation and electroreduction of glucose, J. Electrochem. Soc. 132 (1985), https://doi.org/10.1149/1.2114229.
[30] K. Park, P.N. Pintauro, M.M. Baizer, K. Nobe, Current efficiencies and regeneration of poisoned raney nickel in the electrohydrogenation of glucose to sorbitol, J. Appl. Electrochem. 16 (1986), https://doi.org/10.1007/BF01006542.
[31] A. bin Kassim, C.L. Rice, A.T. Kuhn, Formation of sorbitol by cathodic reduction of glucose, J. Appl. Electrochem. 11 (1981), https://doi.org/10.1007/BF00610988.
[32] P.N. Pintauro, D.K. Johnson, K. Park, M.M. Baizer, K. Nobe, The paired electrochemical synthesis of sorbitol and gluconic acid in undivided flow cells. I, J. Appl. Electrochem. 14 (1984), https://doi.org/10.1007/BF00618739.
[33] Y. Kwon, M.T.M. Koper, Electrocatalytic hydrogenation and deoxygenation of glucose on solid metal electrodes, ChemSusChem 6 (2013), https://doi.org/10.1002/cssc.201200722.
[34] A. Jokic, N. Ristic, M.M. Jaksic, M. Spasojevic, N. Krstajic, Simultaneous electrolytic production of xylitol and xylonic acid from xylose, J. Appl. Electrochem. 21 (1991), https://doi.org/10.1007/BF01020216.
[35] J.A. Lopez-Ruiz, E. Andrews, S.A. Akhade, M.S. Lee, K. Koh, U. Sanyal, S.F. Yuk, A. J. Karkamkar, M.A. Derewinski, J. Holladay, V.A. Glezakou, R. Rousseau, O. Y. Gutiérrez, J.D. Holladay, Understanding the role of metal and molecular structure on the electrocatalytic hydrogenation of oxygenated organic compounds, ACS Catal. 9 (2019), https://doi.org/10.1021/acscatal.9b02921.
[36] U. Sanyal, J. Lopez-Ruiz, A.B. Padmaperuma, J. Holladay, O.Y. Gutiérrez, Electrocatalytic hydrogenation of oxygenated compounds in aqueous phase, Org. Process Res. Dev. 22 (2018), https://doi.org/10.1021/acs.oprd.8b00236.
[37] U. Sanyal, K. Koh, L.C. Meyer, A. Karkamkar, O.Y. Gutiérrez, Simultaneous electrocatalytic hydrogenation of aldehydes and phenol over carbon-supported metals, J. Appl. Electrochem. 51 (2021), https://doi.org/10.1007/s10800-020-01464-7.
[38] A.S. May, E.J. Biddinger, Strategies to control electrochemical hydrogenation and hydrogenolysis of furfural and minimize undesired side reactions, ACS Catal. 10 (2020), https://doi.org/10.1021/acscatal.9b05531.
[39] K.E. Toghill, R.G. Compton, Electrochemical non-enzymatic glucose sensors: a perspective and an evaluation, Int. J. Electrochem. Sci. 5 (2010).
[40] A. Heller, B. Feldman, Electrochemical glucose sensors and their applications in diabetes management, Chem. Rev. 108 (2008), https://doi.org/10.1021/cr068069y.
[41] A. Brouzgou, P. Tsiakaras, Electrocatalysts for glucose electrooxidation reaction: a review, Top. Catal. 58 (2015), https://doi.org/10.1007/s11244-015-0499-1.
[42] J.P. Oña, R.-M. Latonen, N. Kumar, M. Peurla, I. Angervo, H. Grénman, Electrocatalytic hydrogenation of glucose and xylose using carbon fiber supported Au nanocatalysts, Electrochim. Acta 426 (2022), 140754, https://doi.org/10.1016/j.electacta.2022.140754.
[43] L. Prati, G. Martra, New gold catalysts for liquid phase oxidation, Gold Bull. 32 (1999), https://doi.org/10.1007/BF03216617.
[44] O.A. Simakova, A.R. Leino, B. Campo, P. Mäki-Arvela, K. Kordás, J.P. Mikkola, D. Y. Murzin, Linoleic acid isomerization over mesoporous carbon supported gold catalysts, Catal. Today 150 (2010), https://doi.org/10.1016/j.cattod.2009.07.065.
[45] V.B. Fenelonov, V.A. Likholobov, A.Y. Derevyankin, M.S. Mel'gunov, Porous carbon materials prepared from C1-C3 hydrocarbons, Catal. Today 42 (1998), https://doi.org/10.1016/S0920-5861(98)00112-6.
[46] V.v. Sychev, S.v. Baryshnikov, I.P. Ivanov, M.N. Volochaev, O.P. Tarana, Hydrogenation of levulinic acid to γ-valerolactone in the presence of ru-containing catalysts based on carbon material "Sibunit, J. Siberian Federal University: Chemistry 14 (2021), https://doi.org/10.17516/1998-2836-0211.
[47] E.M. Moroz, S.v. Bogdanov, V.A. Likholobov, Structural and substructural parameters of carbon supports sibunit and altunit, Reaction Kinetics Catalysis Lett. 47 (1992), https://doi.org/10.1007/BF02137666.
[48] G.v. Plaksin, O.N. Baklanova, A.v. Lavrenov, V.A. Likholobov, Carbon materials from the Sibunit family and methods for controlling their properties, Solid Fuel Chem. 48 (2014), https://doi.org/10.3103/S0361521914060032.
[49] E.S. Lokteva, V.v. Lunin, E.v. Golubina, V.I. Simagina, M. Egorova, I.v. Stoyanova, C-C bond formation during hydrodechlorination of CCl4 on Pd-containing catalysts, Stud. Surf. Sci. Catal. 130 C (2000), https://doi.org/10.1016/S0167-2991(00)80761-2.
[50] E. Behravesh, N. Kumar, Q. Balme, J. Roine, J. Salonen, A. Schukarev, J. P. Mikkola, M. Peurla, A. Aho, K. Eränen, D.Y. Murzin, T. Salmi, Synthesis and characterization of Au nano particles supported catalysts for partial oxidation of ethanol: influence of solution pH, Au nanoparticle size, support structure and acidity, J. Catal. 353 (2017), https://doi.org/10.1016/j.jcat.2017.07.014.
[51] V.A. Yaylayan, A.A. Ismail, Investigation of the enolization and carbonyl group migration in reducing sugars by FTIR spectroscopy, Carbohydr. Res. 276 (1995), https://doi.org/10.1016/0008-6215(95)00188-Y.
[52] J.C. Speck, The Lobry De Bruyn-Alberda Van Ekenstein transformation, Adv. Carbohydr. Chem. 13 (1958), https://doi.org/10.1016/S0096-5332(08)60352-5.
[53] I.T. Bae, E. Yeager, X. Xing, C.C. Liu, In situ infrared studies of glucose oxidation on platinum in an alkaline medium, J. Electroanal. Chem. 309 (1991), https://doi.org/10.1016/0022-0728(91)87009-S.
[54] I.T. Bae, X. Xing, C.C. Liu, E. Yeager, In situ Fourier transform infrared reflection absorption spectroscopic studies of glucose oxidation on platinum in acid, J. Electroanal. Chem. (1990) 284, https://doi.org/10.1016/0022-0728(90)85043-5.
[55] K. Kunimatsu, T. Senzaki, G. Samjeské, M. Tsushima, M. Osawa, Hydrogen adsorption and hydrogen evolution reaction on a polycrystalline Pt electrode studied by surface-enhanced infrared absorption spectroscopy, Electrochim. Acta 52 (2007), https://doi.org/10.1016/j.electacta.2006.12.007.
[56] J. Lessard, G. Belot, Y. Couture, S. Desjardins, C. Roy, The use of hydrogen generated at the electrode surface for electrohydrogenation of organic compounds, Int. J. Hydrogen Energy 18 (1993), https://doi.org/10.1016/0360-3199(93)90122-Q.
[57] S. Fei, J. Chen, S. Yao, G. Deng, L. Nie, Y. Kuang, Electroreduction of α-glucose on CNT/graphite electrode modified by Zn and Zn-Fe alloy, J. Solid State Electrochem. 9 (2005), https://doi.org/10.1007/s10008-004-0585-y.
[58] Z. Liang, M.A. Villalba, G. Marcandalli, K. Ojha, A.J. Shih, M.T.M. Koper, Electrochemical Reduction of the Simplest Monosaccharides: Dihydroxyacetone and Glyceraldehyde, ACS Catal 10 (2020), https://doi.org/10.1021/acscatal.0c04131.
[59] Y. Sugano, R.M. Latonen, M. Akieh-Pirkanniemi, J. Bobacka, A. Ivaska, Electrocatalytic oxidation of cellulose at a gold electrode, ChemSusChem 7 (2014), https://doi.org/10.1002/cssc.201402139.
[60] G. Moggia, J. Schalck, N. Daems, T. Breugelmans, Two-steps synthesis of D-glucaric acid via D-gluconic acid by electrocatalytic oxidation of D-glucose on gold electrode: Influence of operational parameters, Electrochim. Acta 374 (2021), https://doi.org/10.1016/j.electacta.2021.137852.
[61] A.T. Governo, L. Proença, P. Parpot, M.I.S. Lopes, I.T.E. Fonseca, Electro-oxidation of D-xylose on platinum and gold electrodes in alkaline medium, Electrochim. Acta (2004) 49, https://doi.org/10.1016/j.electacta.2003.11.013.
[62] C. Megías-Sayago, J.L. Santos, F. Ammari, M. Chenouf, S. Ivanova, M.A. Centeno, J. A. Odriozola, Influence of gold particle size in Au/C catalysts for base-free oxidation of glucose, Catal. Today 306 (2018), https://doi.org/10.1016/j.cattod.2017.01.007.
[63] S. Biella, G.L. Castiglioni, C. Fumagalli, L. Prati, M. Rossi, Application of gold catalysts to selective liquid phase oxidation, Catal. Today (2002), https://doi.org/10.1016/S0920-5861(01)00476-X.

[64] S. Biella, L. Prati, M. Rossi, Selective oxidation of D-glucose on gold catalyst, J. Catal. 206 (2002), https://doi.org/10.1006/jcat.2001.3497.
[65] M. Comotti, C. della Pina, R. Matarrese, M. Rossi, The catalytic activity of "naked" gold particles, Angewandte Chemie - International Edition (2004) 43, https://doi.org/10.1002/anie.200460446.
[66] J. Ma, Z. Liu, J. Song, L. Zhong, D. Xiao, H. Xi, X. Li, R. Sun, X. Peng, Au@: H -Al2O3 analogic yolk-shell nanocatalyst for highly selective synthesis of biomass-derived d-xylonic acid via regulation of structure effects, Green Chem. 20 (2018), https://doi.org/10.1039/c8gc02618a.
[67] X. Meng, Z. Li, D. Li, Y. Huang, J. Ma, C. Liu, X. Peng, Efficient base-free oxidation of monosaccharide into sugar acid under mild conditions using hierarchical porous carbon supported gold catalysts, Green Chem. 22 (2020), https://doi.org/10.1039/c9gc04333k.
[68] B. Zhou, J. Song, Z. Zhang, Z. Jiang, P. Zhang, B. Han, Highly selective photocatalytic oxidation of biomass-derived chemicals to carboxyl compounds over Au/TiO2, Green Chemistry. 19 (2017). 10.1039/c6gc03022j.